Organic field-effect transistors based on tetrathiafulvalene derivatives*

Xike Gao, Wenfeng Qiu, Yunqi Liu‡, Gui Yu, and Daoben Zhu

Beijing National Laboratory for Molecular Sciences, Key Laboratory of Organic Solids, Institute of Chemistry, Chinese Academy of Sciences, Beijing 100080, China

Abstract: In recent years, tetrathiafulvalene (TTF) and its derivatives have been used as semi-conducting materials for organic field-effect transistors (OFETs). In this review, we summarize the recent progress in the field of TTF-based OFETs. We introduce the structure and operation of OFETs, and focus on TTF derivatives used in OFETs. TTF derivatives used in OFETs can be divided into three parts by the semiconductor's morphology and the device fabrication technique: (1) TTF derivatives used for single-crystal OFETs, (2) TTF derivatives used for vacuum-deposited thin-film OFETs, and (3) TTF derivatives used for solution-processed thin-film OFETs. The single-crystal OFETs based on TTF derivatives were fabricated by drop-casting method and showed high performance, with the mobility up to 1.4 cm^2/Vs. The vacuum-deposited thin-film OFETs based on TTF derivatives were well developed, some of which have shown high performance comparable to that of amorphous silicon, with good air-stability. Although the mobilities of most solution-processed OFETs based on TTF derivatives are limited at 10^{-2} cm^2/Vs, the study on solution-processable TTF derivatives and their devices are promising, because of their low-cost, large-area-coverage virtues. The use of organic charge-transfer (OCT) compounds containing TTF or its derivatives in OFETs is also included in this review.

Keywords: tetrathiafulvalene derivatives; organic field-effect transistors; single crystals; thin films; semiconductors.

INTRODUCTION

Organic field-effect transistors (OFETs) have attracted more and more attention in the field of organic electronics due to their virtues of low cost, large-area coverage, mechanical flexibility, light weight, and compatibility with plastic substrates over their inorganic counterparts [1–4]. Applications for OFETs are promising, such as circuits, flexible displays, radio frequency identification (RF-ID) tags, sensors, and memories [5,6]. Organic semiconductors are the key components of OFETs. They can be basically classified into acene- and/or thiophene-fused aromatic compounds, oligothiophenes and their co-oligomers, polythiophenes, aromatic bisimides, metal phthalocyanines, fullerenes, and tetrathiafulvalene (TTF) derivatives. TTF and its derivatives, as electron donors in organic charge-transfer (OCT) materials or organic radical salts, have been intensively investigated in the field of organic conductors and superconductors [7,8]. On the other hand, TTF derivatives have some good features for

acting as semiconducting layers in OFETs: (1) they are mostly achieved by simple synthetic paths and are easily chemically modified; (2) they are generally soluble in common solvents and benefit the solution-processable devices; (3) the planar molecular conformation and the strong intermolecular interactions in the solid-state induced by $\pi\cdots\pi$ stacking and $S\cdots S$ interactions; and (4) the good electron donor ability with highest occupied molecular orbital (HOMO) levels close to the work function of usual metallic electrodes, affording little energy barrier for charge injection from metal electrodes into their active layers [9,10].

Bourgoin et al. reported the first TTF-based OFET in which the Langmuir–Blodgett layers of TTF derivative (**1**, Scheme 1) was the active channel [11]. The device behaved as a *p*-type transistor in the depletion mode. Tanaka and coworkers prepared OFETs using the donor compound (**2**, Scheme 1) and its stacked layers with the acceptor tetracyanoquinodimethane (TCNQ) as the semiconducting channel [12]. The early work on TTF-based OFETs did not attract much attention due to the poor FET performance. Only recently, TTF derivatives have attracted considerable attention for their application in OFETs [9]. A high-mobility OFET (1.4 cm^2/Vs) has been reported using single crystals of dithiophene-TTF (**3** Scheme 2) as the active layer [13], and a thin-film transistor based on dichloroquinoxalino-pyrazino-TTF (**23**, Scheme 3) showed high mobility of 0.64 cm^2/Vs, with the on/off current ratio of 10^5–10^6 [14]. Rovira and Mas-Torrent have written a review about the TTF-based OFETs, the review involved the works up to 2005 [9]. In the last two years, there has been notable new progress in this field. The purpose of this review is to display a comprehensive development in the field of TTF-based OFETs. This review will introduce the structure and operation of OFETs and focus on TTF derivatives used in OFETs. The TTF derivatives can be divided into three parts by their morphology and the device fabrication technique: (1) TTF derivatives used for single-crystal OFETs, (2) TTF derivatives used for vacuum-deposited thin-film OFETs, and (3) TTF derivatives used for solution-processed thin-film OFETs. In particular, the design and synthesis of new TTF derivatives for high-performance OFETs were highlighted. The use of OCT compounds containing TTF or its derivatives in OFETs is also included in this review. Finally, the prospects and problems that exist in TTF-based OFETs are discussed.
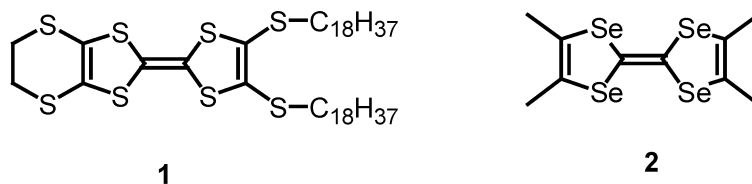
**Scheme 1** The early used TTF derivatives for OFETs.
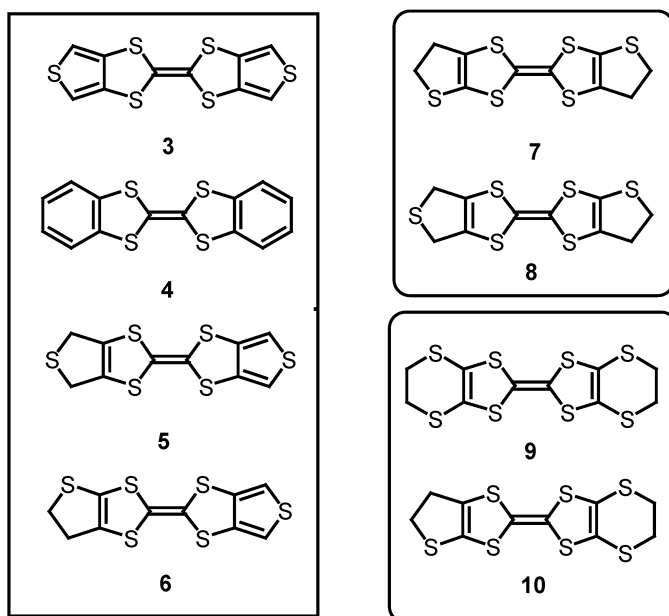
Scheme 2 TTF derivatives used for single-crystal OFETs.
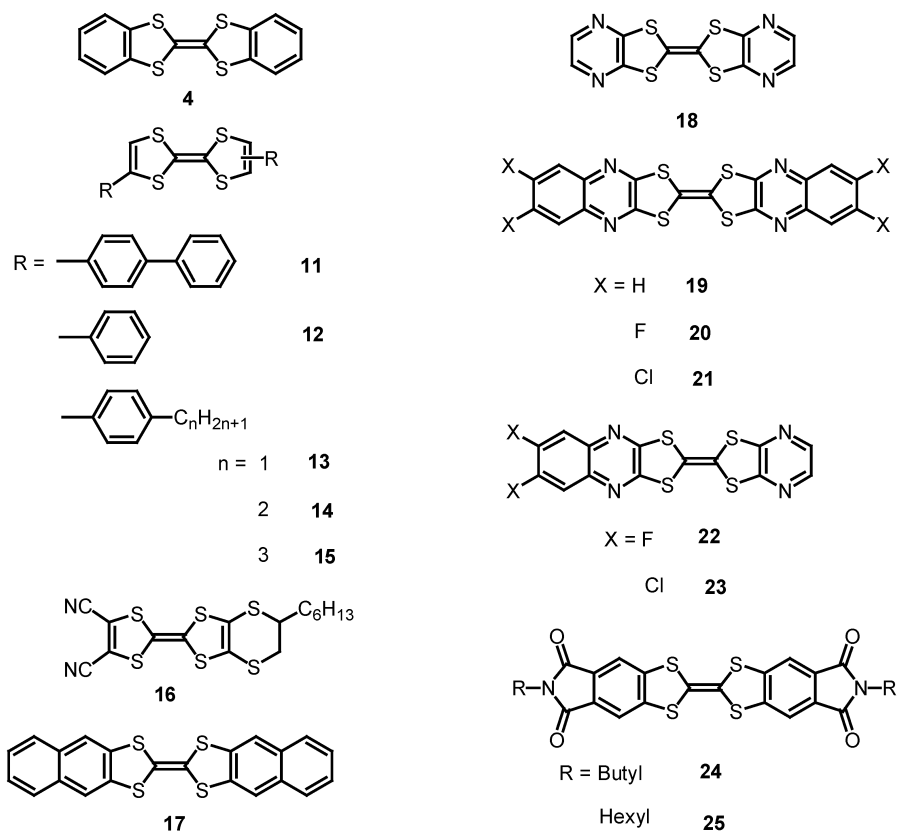
Scheme 3 TTF derivatives used for vacuum-deposited thin-film OFETs.

OFET STRUCTURE AND OPERATION

A thin-film OFET device consists of a gate electrode, a dielectric insulator, an organic semiconducting film deposited on a gate/insulator substrate, and two metallic electrodes (drain and source) contacted with the semiconductor. There are two types of OFET structures, the top-contact (TC) and bottom-contact (BC) electrode geometries. In the TC case (Fig. 1), the organic film is deposited first, followed by the drain and source electrodes deposited by metal evaporation through a shadow mask. In the BC case, the deposition sequence is reversed. The current (I_{DS}) flow between the drain and source electrodes is modulated by an applied gate voltage (V_G). When no V_G is applied, the drain current is very low if the semiconductor is not highly doped, and the transistor lies at the off-state. With an increase of V_G, a layer of mobile charges can accumulate at the interface between the semiconductor and insulator. Then, the current is increased due to the accumulated charge carriers and the transistor is at the on-state. The current flow (I_{DS}) can also be modulated by the drain/source voltage (V_{DS}). As shown in Fig. 2a, the current that flows from the source to the drain electrode (I_{DS}) under a given V_G increases almost linearly with the increasing V_{DS} and gradually becomes saturated.
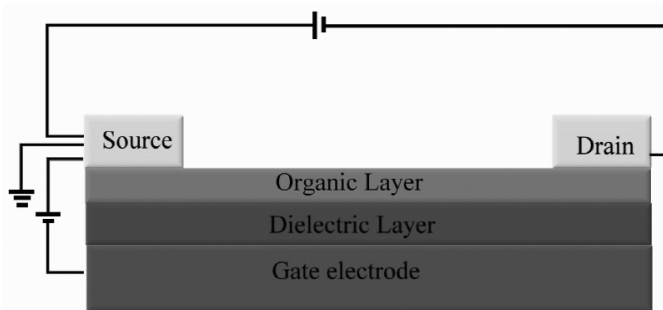

Fig. 1 Schematic diagram of TC OFET.

OFETs are typically characterized by two ways, one is by holding V_G constant and sweeping V_{DS} (commonly referred to as I_{DS}–V_{DS} or output curves, Fig. 2a); the other is by holding V_{DS} constant and sweeping V_G (commonly referred to as I_{DS}–V_G or transfer characteristics, Fig. 2b). When an OFET is active, upon the application of negative V_G and V_{DS}, the organic semiconductor is named as p-channel because holes are the majority charge carriers. On the other hand, when a positive I_{DS} is observed upon the use of positive V_G and V_{DS}, the semiconductor is n-channel for the electrons are charge carriers. In a few cases, OFETs operate for both V_G and V_{DS} polarities and the semiconductor is said to be ambipolar. The current I_{DS} modulated by V_G is approximately determined from the following equations [15]:

$$I_{DS} = (W/L)C_i\mu(V_G - V_T)V_{DS} \qquad \text{(linear regime)} \qquad (1)$$

$$I_{DS} = (W/2L)C_i\mu(V_G - V_T)^2 \qquad \text{(saturation regime)} \qquad (2)$$

where I_{DS} is the drain/source current, μ is the field-effect mobility, W is the channel width, L is the channel length, C_i is the capacitance per unit area of the gate dielectric layer, and V_T is the threshold voltage at which the current starts to rise. The most critical properties of an OFET device are the charge mobility and on/off current ratio. The charge mobility quantifies the average charge-carrier drift velocity per unit electric field, whereas the on/off current ratio is defined as the drain/source current ratio between the on- and off-states. In the saturation regime, we often used eq. 2 to estimate the charge-carrier mobility. For an organic semiconductor, to be used in optoelectronic devices such as active matrix displays that require sharp turn-on and fast switching, charge mobilities >0.1 cm^2/Vs and an on/off current ratio >10^6 are needed [16].
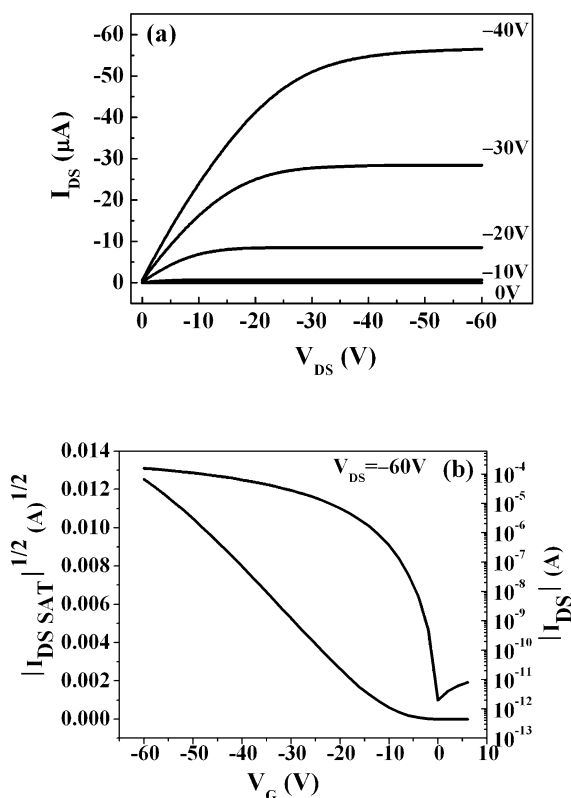
Fig. 2 (a) Example I_{DS}–V_{DS} curves for a pentacene thin-film FET for various values of V_G. (b) Example I_{DS}–V_G curves plotted on semilogarithmic axes for the same device for various values of V_{DS}. The $I^{1/2}$ vs. V_G for V_{DS} = –60 V is shown on the left-hand axis.

TTF DERIVATIVES FOR OFETs

In recent years, TTF derivatives have been used in OFETs in different morphologies (single-crystal and thin-film) and by various fabrication techniques (drop-casting, vacuum evaporation, spin-coating, and zone-casting). On the one hand, the study in the field of organic conductors and superconductors afforded a great deal of TTF derivatives, some of which have been studied in OFETs. On the other hand, some new semiconducting TTF derivatives with novel structures and properties have been and are being designed and synthesized for high-performance OFETs.

TTF derivatives for single-crystal OFETs

Single crystals of organic semiconductors offer a good way to investigate charge transport as function of molecular property and arrangement [17]. Although there are many difficulties associated with the application of single-crystalline OFETs, a recent report on "patterning organic single-crystal transistor arrays" by Bao et al. constitutes a promising step that might ultimately allow us to utilize high-performance single-crystal OFETs for large-area flexible electronics applications [18]. The research work on single-crystal TTF-based OFETs was done by Rovira and Mas-Torrent [13,19–22]. As shown in Scheme 2, eight TTF derivatives (**3–10**) were used as semiconducting layer for single-crystal OFETs. Their FET characteristics are summarized in Table 1. All the devices were fabricated by using a simple-solution, drop-casting method.

Table 1 Charge-carrier mobilities (μ), maximum transfer integrals of the symmetric derivatives (t_{max}), and isolated molecular reorganization energies of TTF derivatives (**3–10**) using the neutral local minimum energy conformation best approximating the crystal structure conformation (λ_{reorg}).

TTF derivative	μ, cm^2/Vs	λ_{reorg}, eV	t_{max}, eV	References
3	0.01–1.4	0.238	0.034	[19]
4	0.01–1.0	0.248	0.037	[20]
5	0.01–0.37	0.258		[19]
6	0.01–0.12	0.238		[19]
7	0.001–0.05	0.246	0.021	[19]
8	8×10^{-4}–3×10^{-3}	0.314		[19]
9	1×10^{-5}–5×10^{-3}	0.550	0.019	[19]
10	2×10^{-5}–3×10^{-4}	0.488		[19]

The devices based on **3** showed the highest FET performance with the mobilities up to 1.4 cm^2/Vs [13]. It is this work that promotes the development of TTF-based OFETs. The crystal packing of **3** is similar to that of pentacene, giving a herringbone pattern, with the short interplanar distance (3.56 Å) and intermolecular S···S interactions (3.6 Å). Density functional theory (DFT) calculations afforded a stable HOMO level of **3** (–5.123 eV) [10], which is equal to the work function of gold (5.1 eV) [23]. The densely herringbone packing, the stable HOMO level, and the little charge-injection energy barrier all contribute to the high FET performance of **3**. Like **3**, dibenzo-TTF (DB-TTF) (**4**) is well soluble in organic solvents and its single crystals form uniform stacks of almost planar molecules in a herringbone pattern. In addition, the calculated HOMO energy levels (~ –4.9 eV), transfer integral values (0.238 and 0.248 eV), and reorganization energy values (0.034 and 0.037 eV) for **3** and **4**, respectively, are very similar. All the above results indicate that it is possible to prepare good-quality DB-TTF crystals with high FET mobilities. The single-crystal FET devices based on **4** showed high hole mobilities in the range of 0.01–1.0 cm^2/Vs [20]. However, there were some drawbacks for their FET characteristics, such as large off-current at zero V_G (i.e., the existence of rich carriers in the active layer under zero V_G) and the lack of saturation currents in the output curves.

Correlation between crystal structure and mobility in OFETs based on **3–10** were studied in detail [19,20]. The results showed two features: (1) the herringbone crystal structure (**3–6**) displayed the best FET performance, the off-set face-to-face stacking structure (**7** and **8**) afforded the moderate mobilities, and the discrete dimer-stacking structure (**9** and **10**) gave the worst FET properties; (2) for the same stacking pattern, the mobility of symmetric compound was bigger than that of unsymmetric one, and the bigger molecular disorder led to the lower FET mobility.

Transfer integral (*t*) and reorganization energy (λ_{reorg}) are two major parameters to determine charge mobility: the transfer integral needs to be maximized, and the reorganization energy should be small for efficient charge transport [24]. DFT calculations were carried out by Bromley and Mas-Torrent to estimate transfer integral and reorganization energy of compounds **3–10** [19,20,25]. The results are included in Table 1. Compounds **3–6** showed the planar neutral molecular conformation induced by the steric constraint of the herringbone crystal packing. Their reorganization energy for an isolated planar molecule was small (<0.260 eV). It should be noted that local intermolecular interactions have a strong influence on λ_{reorg} values, and the embedded molecule has a much lower λ_{reorg} value [25]. For the embedded molecule of **3**, a λ_{reorg} was only 0.042 eV, which is on the same order of that of pentacene (0.080 eV) [25]. The DFT results would help to explain the high mobility reported for single-crystal OFETs based on **3–6**.

TTF derivatives for thin-film OFETs

The aforementioned single-crystal devices based on TTF derivatives were fabricated by simple-solution, drop-casting method and showed high FET performance. However, there are many difficulties associated with the applications of single-crystal OFETs [26]. For example, the growth of large-area-coverage single crystals of organic materials is challenging. In addition, the resulting crystals are usually very brittle, and it is difficult to form electrical contact with the crystal without damaging it or introducing charge traps at interfacial sites. Therefore, organic single-crystal materials could find use as models to study charge transport, rather than being used for industrial purposes. As compared with their single-crystal devices, thin-film OFETs based on TTF derivatives would be promising for industrial applications.

TTF derivatives for vacuum-deposited thin-film OFETs

TTF derivatives having big rigidity π–conjugations are mostly insoluble or less soluble in most common solvents due to the strong π–interactions and/or the lack of flexible chains. Thus, the use of vacuum sublimation is required to fabricate their thin-film OFET devices, although this processing technique is expensive and time-consuming. For a same soluble semiconducting small organic compound, comparing with the solution process, the vacuum-deposited technique usually fabricates higher-quality thin film and affords higher FET performance. Scheme 3 exhibits the TTF derivatives used for vacuum-deposited thin-film OFETs. Their FET characteristics are summarized in Table 2.

Table 2 FET characteristics of vacuum-deposited thin-film devices based on TTF derivatives **4** and **11–25**.

Compound	Device geometry	T_{sub} (°C)	Mobility (cm^2/Vs)	On/off ratio	HOMO (eV)	References
4	BC	RT	0.06	10^4		[27]
	BC	RT	0.012	7	–4.9	[29]
	TC	RT	10^{-3}	10^2		[28]
11	BC	RT	0.11	10^2	~ –4.8	[29,30]
12	BC	RT	2×10^{-5}	5	~ –4.8	[29]
13	BC	RT	3×10^{-4}	2	~ –4.8	[29]
14	BC	RT	1.0×10^{-4}	1.02	~ –4.8	[29]
15	BC	RT	3×10^{-6}	10	~ –4.8	[29]
16	TC	RT	0.007–0.02			[31]
17	BC	RT	0.38	1.6×10^2		[27]
	BC	80	0.22	3.0×10^2		[27]
	TC	RT	0.42	6.0×10^3		[27]
18	BC	RT	3.3×10^{-5}	10^6		[27]
19	BC	RT	1.0×10^{-4}	10^6		[27]
	BC	80	0.08	10^4	–5.38	[27]
	TC	80	0.2	10^6		[27]
20	TC	RT	0.10 (*n*-type)	1.5×10^5	–5.83	[14]
21	TC	RT	0.11 (*n*-type)	1.0×10^6	–5.84	[14]
22	TC	RT	0.20	4.0×10^5	–5.70	[14]
23	TC	RT	0.64	3.3×10^5	–5.75	[14]
24	TC	RT	0.011–0.094	10^6–10^8	–5.46	[28]
25	TC	RT	0.12–0.40	10^6–10^8	–5.42	[28]

Yamashita and coworkers first reported the thin-film OFET devices based on DB-TTF (DB-TTF, **4**) [27]. The BC devices showed mobility up to 0.06 cm^2/Vs, with the current on/off ratio of 10^4.

However, the following studies on thin-film devices based on **4** by Mori et al. and by our group showed very poor FET performance, such as the low mobility, small on/off ratio, large off-current, and the lack of saturation current [28,29]. The reason might be attributed to the different measurement conditions. The poor FET performance was also found in the thin-film devices based on compounds **11–16** [29–31]. Similar to **4**, these compounds have high HOMO levels, their thin films are labile to oxygen, and the resulting dopants increase the conductivity of the film in the off- or ungated-state and lead to aforementioned poor FET performance. To enhance the air stability of TTF derivatives, Yamashita and coworkers took the following measures: (1) introducing fused aromatic rings (benzene, naphthalene, pyrazine, or quinoxaline rings) to TTF skeleton, (2) further attaching electron-withdrawing halogen groups (F or Cl) onto the fused TTF skeleton, and obtaining high-performance TTF-based FET devices [13,27]. TTF derivatives **17–23** were studied in detail by Yamashita et al. for thin-film OFETs, including the relationship between their FET characteristics and crystal structures.

Devices based on dinaphtho-TTF (**17**) showed high mobility up to 0.42 cm^2/Vs with the on/off ratio on the order of 10^2–10^4 [27]. Similar to **4**, **17** has the herringbone-type crystal structure. However, the mobility of **17** was much higher than that of **4** due to its π-expanded structure that benefits the intermolecular π–π interactions. The first oxidation potential of **19** (1.15 V) was much higher than that of **17** (0.72 V), which led to its high oxygen stability and high current on/off ratios (up to 10^6) (under the 760 Torr of O_2 pressure, the mobility was little increased and the off-current was unchanged) [27]. When four halogen atoms (F or Cl) were attached to the skeleton-ends of **19**, the new compounds **20** and **21**, having the low-lying lowest unoccupied molecular orbital (LUMO) levels (–3.62 eV and –3.81 eV, respectively), showed *n*-type FET characteristics in their thin-film devices [14]. Because of the presence of intermolecular charge-transfer interactions between the donor and acceptor units, **19–21** displayed the strong face-to-face stacking crystal structure, with the short interplanar distances ranging from 3.31 to 3.44 Å. The intermolecular charge transfer might benefit the high charge mobility (up to 0.20 cm^2/Vs) due to the fortified intermolecular π-stacking. TTF derivatives **22** and **23** have one pyrazine and one halogen-substituted quinoxaline units, affording the unsymmetrical molecular structure, but their thin-film devices displayed even high *p*-type FET performance with the mobility up to 0.64 cm^2/Vs [14].

Up to now, most TTF-based thin-film OFETs fabricated by vacuum evaporation either showed poor performance in air due to oxygen-doping or displayed high performance but measured in vacuum, and little work was done to investigate the stability of TTF-based OFETs. We have developed a new type of TTF/bisimide derivatives, DB-TTF bisimides (**24** and **25**), using a facile and general synthetic strategy [28]. The synthetic strategy of DB-TTF bisimides was shown in Scheme 4. Compounds **24** and **25** have the planar π-expanded molecular structure and the lower-lying HOMO levels (–5.4 eV) relative to that of DB-TTF (**4**) (–4.97 eV) [28]. For **24** and **25**, the low-lying HOMO level benefits the stability to oxygen, and the columnar intermolecular π-stacking with the intercolumnar S···S and S···O interactions contribute to the charge transport. The thin-film FET devices based on **24** and **25** were fabricated at room temperature and measured in air, showing high mobility up to 0.094 cm^2/Vs (average 0.033 cm^2/Vs) and 0.40 cm^2/Vs (average 0.22 cm^2/Vs), respectively, with even high on/off ratio on the order of 10^6–10^8. The values of devices based on **25** are comparable to the mobilities (0.1–1 cm^2/Vs) and on/off ratios (>10^6) exhibited by amorphous silicon thin-film transistors that are widely used for driving circuits in liquid crystal display. It should be noted that these thin-film devices exhibited good reproducibility and air-stability. Figure 3 showed the FET characteristics of a device based on **25**. The air-stability test of devices based on **24** and **25** is displayed in Fig. 4. The planar π-expanded molecular structure, easily chemical modification, high thermal- and air-stability, and excellent charge-transport property make DB-TTF bisimides promising organic electronic materials.
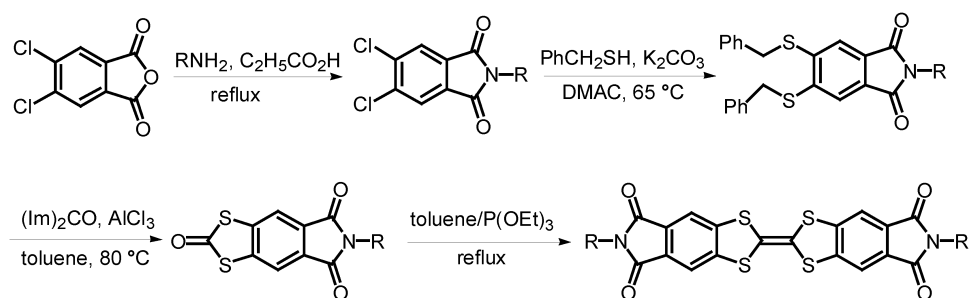
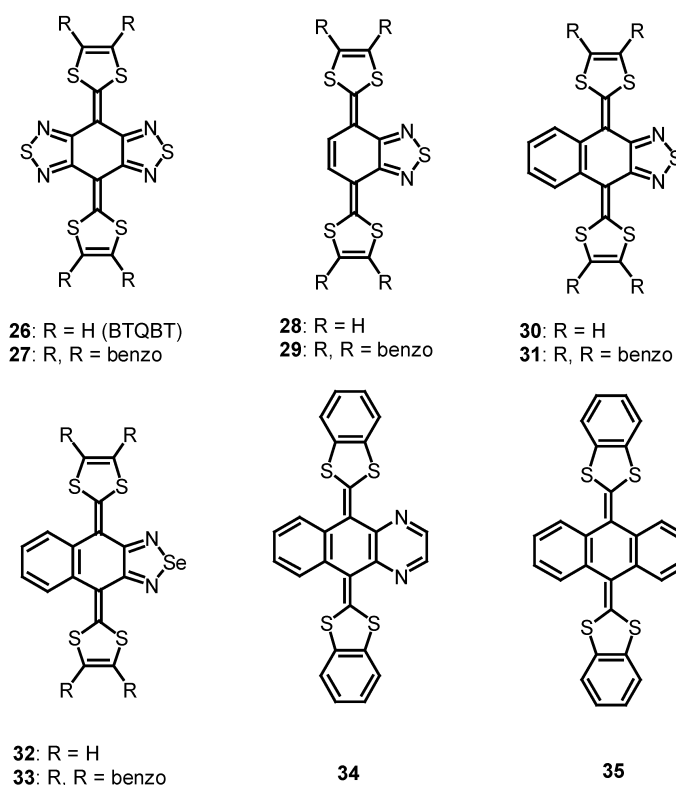**Scheme 4** The synthetic strategy of DB-TTF bisimides. Adapted from ref. [28].
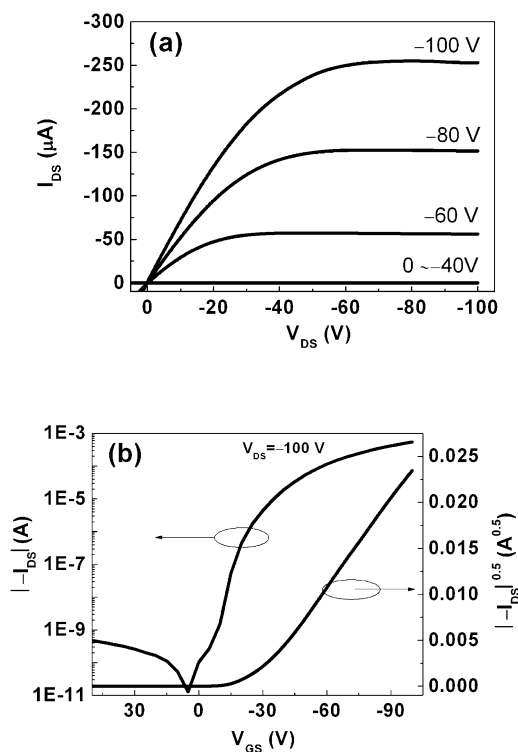
Fig. 3 FET characteristics of a device based on **25** fabricated at room temperature: output characteristics (a) and transfer characteristics at V_{DS} = 100 V (b). Adapted from ref. [28].
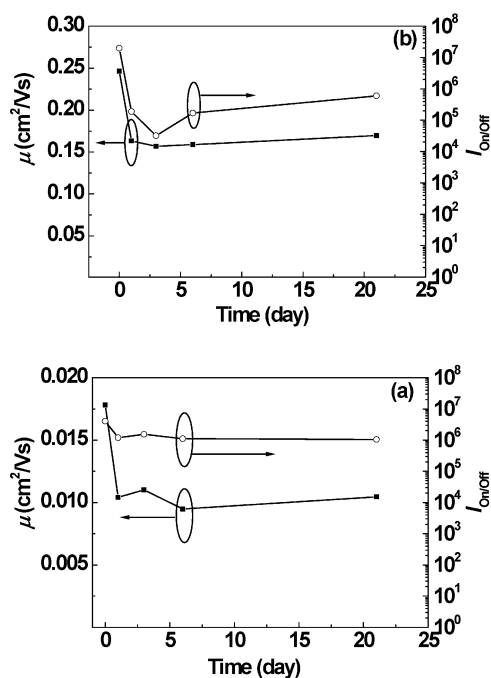
Fig. 4 Mobilities and on/off ratios for a FET device based on **24** (a) or **25** (b) tested over a period of three weeks in air. Adapted from ref. [28].

As shown in Scheme 5, some bis(1,3-dithiol-2-ylidene) compounds (**26–35**) that are π-expanded TTF analogs, like bis[1,2,5]thiadiazolo-*p*-quinobis(1,3-dithiole) (BTQBT), were studied for thin-film OFETs by Forrest and by Yamashita [32–34]. The FET measurements were carried out in vacuum or using another organic layer to isolate semiconductor layer from air. Among the bis(1,3-dithiol-2-ylidene) compounds mentioned above, BTQBT (**26**) attracted more attention because its single crystal showed a high hole mobility of 4 cm^2/Vs [35]. Thin-film FET devices based on **26** showed hole mobilities in the range of 0.02–0.2 cm^2/Vs with on/off ratios of 10^3–10^8 [32–34]. Compounds **27**, **29**, **31**, **33**, and **34** exhibited poor *p*-type FET performance, with the mobilities of 10^{-4}–10^{-7} cm^2/Vs [34]. However, other compounds **28**, **30**, **32**, and **35** did not show FET characteristics due to their strong electron-donating property. The butterfly-shape molecular structure of **35** disturbed efficient intermolecular π–π interactions, which was another reason for no observation FET characteristics [34]. Although bis(1,3-dithiol-2-ylidene) compounds are not air-stable semiconductors and most of them showed poor FET performance, the studies on them further demonstrated that the moderate electron-donating properties of the molecules and efficient intermolecular interactions were essential for FET performance [34].

26: R = H (BTQBT)
27: R, R = benzo

28: R = H
29: R, R = benzo

30: R = H
31: R, R = benzo

32: R = H
33: R, R = benzo

34

35

Scheme 5 π-expanded TTF analogs: bis(1,3-dithiol-2-ylidene) compounds.

TTF derivatives for solution-processed thin-film OFETs

The vacuum-deposited method has been used for fabricating TTF-based thin-film transistors and afforded high-performance FET devices, but this thermal evaporation manufacture is expensive, time-consuming, and limited for obtaining large-area-coverage thin films. To truly realize the low-cost and large-area-coverage aspects of organic electronics, organic semiconductors must be deposited from solution with more economical and versatile techniques, such as spin-coating, zone-casting, ink-jet printing, screen-printing, and stamping [36]. For TTF-based OFETs, this requirement has in turn driven the development of new solution-processable TTF derivatives. An approach to afford solution-processable TTF derivatives is the attachment of flexible side chains or bulky groups to π-skeleton that contains TTF unit. Scheme 6 shows TTF derivatives (**3**, **36–49**) used for solution-processed thin-film OFETs. Several solution-processed techniques were applied for fabricating their thin-film devices, such as drop-casting [37,38], zone-casting [39,40], and spin-coating [41–43]. FET characteristics of thin-film devices based on TTF derivatives (**3**, **36–49**) are summarized in Table 3.
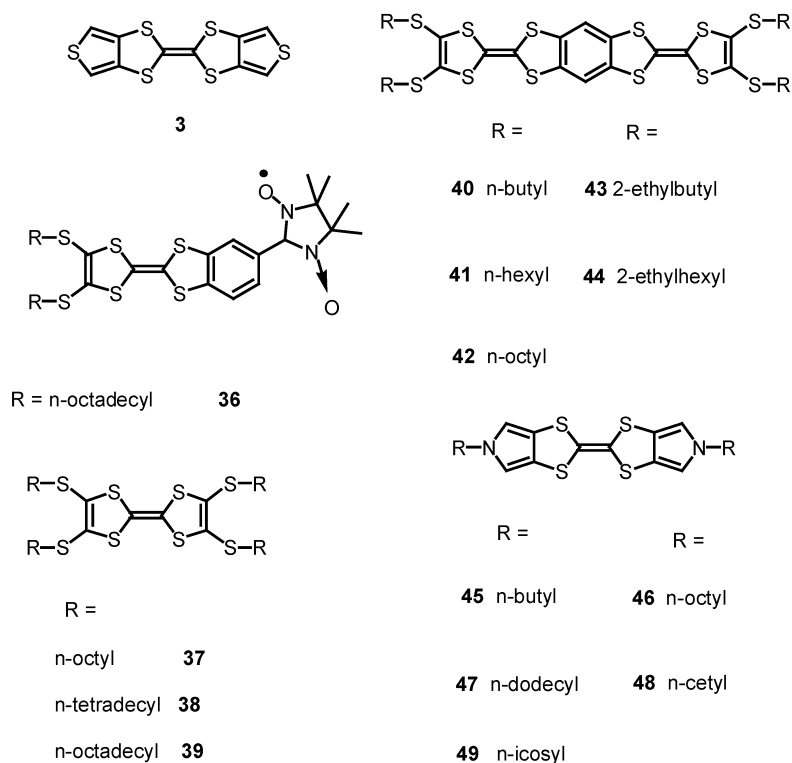
Scheme 6 TTF derivatives for thin-film OFETs fabricated by solution-process.

Table 3 FET characteristics of solution-processed thin-film devices based on TTF derivatives **3** and **36–49**.

Compound	Fabrication method	Device geometry	Mobility (cm^2/Vs)	On/off ratio	References
3	Zone-casting	TC	0.01–0.17		[40]
36	Spin-casting	BC	5×10^{-9}		[37]
37	Drop-casting	BC	3.4×10^{-6}	<2	[38]
38	Drop-casting	BC	1.6×10^{-5}	<2	[38]
39	Drop-casting	BC	2.7×10^{-5}	<2	[38]
	Zone-casting	TC	4×10^{-4}–0.08	10^2–10^4	[39]
40	Spin-coating	TC	5×10^{-3}	10^2	[41]
41	Spin-coating	TC	0.02	10^2	[41]
42	Spin-coating	TC	6.7×10^{-5}	10^3	[41]
43	Spin-coating	TC	4×10^{-5}–1.1×10^{-4}	10^3	[42]
44	Spin-coating	TC	1×10^{-4}–5.6×10^{-4}	10^3–10^4	[42]
45	Spin-coating	TC	1.7×10^{-5}	10	[43]
46	Spin-coating	TC			[43]
47	Spin-coating	TC	6.8×10^{-3}	2×10^2	[43]
48	Spin-coating	TC	0.013	10^4	[43]
49	Spin-coating	TC	0.013	10^4	[43]

Sugawara and coworkers reported thin-film OFETs based on a TTF derivative (**36**) that bears stable organic radical moiety and long alkyl chains [37]. The thin films were fabricated by drop-casting, and following by the melting–freezing method. This is the first observation of FET characteristics for organic radicals, although the mobility is low (5×10^{-9} cm^2/Vs) and the on/off ratio is very small. Our group developed other organic radical-based OFETs using 1-imino nitroxide pyrene as semiconducting active layer [44]. The devices could be operated within low voltage and showed *p*-type FET characteristics with excellent performance (mobility up to 0.1 cm^2/Vs and on/off ratio of nearly 5×10^4). Since the neutral single crystals of tetrakis(alkylthio)-tetrathiafulvalenes (TTC$_n$-TTF) showed rather high conductivity of 10^{-7}–10^{-5} S/cm due to the fastener-effect of long alkyl chains [45], their FET characteristics in thin films are promising. Ukai et al. investigated the transport property of OFETs based on TTC$_n$-TTF derivatives with $n = 8, 14, 18$ (**37–39**) [38]. TTC$_n$-TTF was drop-casted on the prefabricated FET structure from its saturated chloroform solution, affording the BC device geometry. The field-effect hole mobility of 10^{-6}–10^{-5} cm^2/Vs was obtained for compounds **37–39**. The mobility increased with the enhanced length of alkyl chains, which was attributed to the reduction of intermolecular distance between adjacent TTF units caused by the fastener-effect of long alkyl chains. Besides the low mobility, the devices based on **37–39** showed other poor FET characteristics, such as the large off-current at zero V_G, the small on/off ratio (<2), and the non-saturating behavior.

Other than those fabricated by drop-casting [38], thin-film devices based on TTC$_{18}$-TTF (**39**) fabricated by zone-casting method showed clear linear and saturation regions, and much higher FET performance, with the mobility up to 0.08 cm^2/Vs and on/off ratio on the order of 10^4 [39]. The improved FET performance of devices based on **39** might be attributed to its improved high-quality thin films obtained by zone-casting technique. As shown in Fig. 5b, the zone-casting technique is a one-step method for preparing large-area-oriented films of solution-processable materials without using a pre-oriented substrate, which supplies a solution of an organic material through a stationary flat nozzle onto a moving substrate. Using this solution-processed technique, Rovira and coworkers fabricated more than 40 thin-film FET devices based on **39**, these devices showed good reproducibility of their performance. The films were characterized by atomic force microscopy (AFM) and X-ray diffraction (XRD), indicating the formation of lamellar ordering and a high-crystalline quality. The XRD study also demonstrated that molecules of **39** were tilted with respect to the substrate surface and well aligned in the casting direction. The FET mobility measured along the casting direction was about one order of magnitude higher than those determined in the direction perpendicular to the orientation. Furthermore, all the devices after annealing exhibited an enhanced performance with FET mobility about one order of magnitude higher. All the results can be clearly seen from Fig. 6. Recently, Mas-Torrent and Rovira applied zone-casting technique to dithiophene-TTF (**3**) which has low molecular weight and lacks long flexible chains, and obtained a large-area coverage of well-oriented films [40]. OFETs employing these films showed high mobilities with a maximum value of 0.17 cm^2/Vs. This value is about one order of magnitude lower than that of its single-crystal OFETs (1.4 cm^2/Vs) [13], but the fact that large-area coverage of well-oriented films of **3** was prepared from solution makes these devices suitable for low-cost and large-area-coverage electronics.
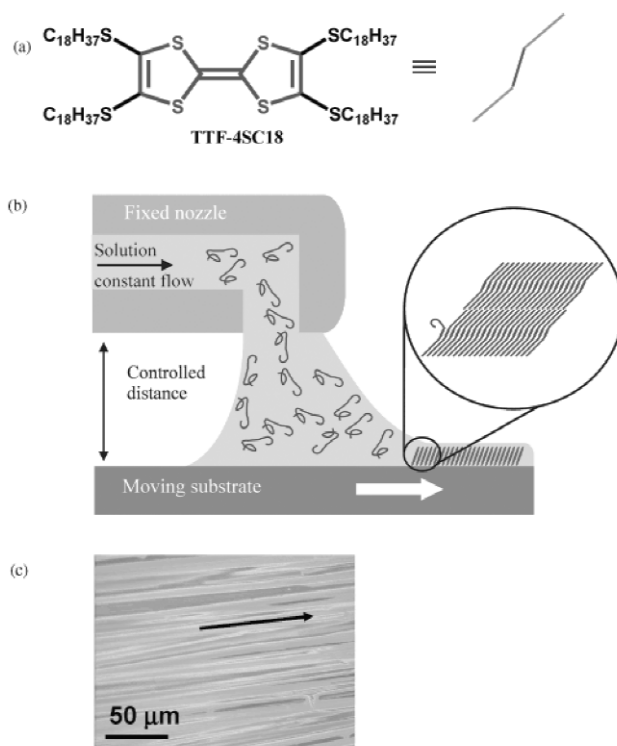
Fig. 5 (a) Molecular structure of tetrakis-(octadecylthio)-tetrathiafulvalene (TTF-4SC18, **39**). (b) Schematic representation of the zone-casting technique. (c) Optical micrograph image of the zone-cast film of **39**. The black arrow indicates the casting direction. Adapted from ref. [39].
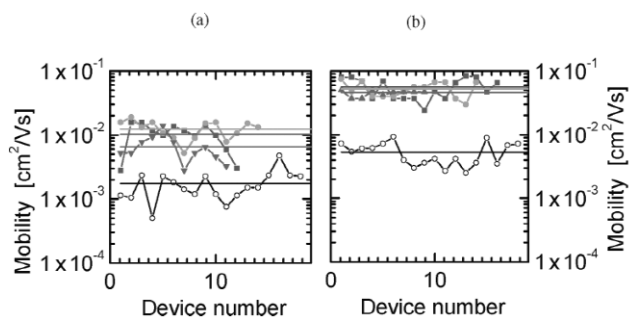

Fig. 6 Field-effect mobilities for a series of FET devices based on the zone-cast TTC_{18}-TTF (**39**) layers on the $SiO_2/Si_3N_4/Si$ substrate with different channel lengths oriented parallel and perpendicular to the casting direction before annealing (a) and after annealing (b). Full symbols show results for the devices with the channel length parallel to the casting direction: squares: $L = 100$ μm; circles: $L = 80$ μm; and triangles: $L = 50$ μm. Open circles show results for the devices with channel length perpendicular to the casting direction, $L = 80$ μm. Adapted from ref. [39].

As shown in Schemes 7 and 8, we developed a new type of benzene-fused bis(TTF) compounds (type B) using a facile synthetic strategy [41,42], which differs from those (type A) synthesized by Müllen and co-workers [46] and by Moradpour et al. [47] applying long difficult synthetic paths. We fabricated thin-film FET devices of linear benzene-fused bis(TTF) compounds (Scheme 6, **40–44**) by spin-coating method, and investigated their FET characteristics (see Table 3). These devices are the first examples of spin-coating thin-film OFETs based on TTF derivatives and of oligomeric TTF-based OFETs. All devices based on bis-TTF compounds **40–44** exhibited *p*-type FET characteristics, of which devices based on **41** (bearing four *n*-hexyl chains) afforded the highest mobility of 0.02 cm^2/Vs [41]. In spite of the high mobility, compound **41** also showed some poor FET characteristics, such as large off-current at zero V_G, low on/off ratio and non-saturating behavior, which also occurred in FET devices based on **40** and **42** that contain *n*-alkyl chains. In comparison with FET performance of **41**, the mobility of compounds **43** and **44** were much lower because the branched chains prohibited the well-ordered packing of molecules, but there were many improved aspects, such as good saturation behavior, much smaller off-current, and higher on/off ratio of 10^3–10^4. Figure 7 shows the output FET characteristics of two devices based on isomeric compounds **41** and **43**, respectively. Compounds **40–42** have much lower solubility relative to that of **43** and **44**, which led to their poor spin-coated thin films. The strong molecular fastener effect induced by the *n*-alkyl chains resulted in the high-conducting thin films of **40–42** (10^{-6}–10^{-4} S/cm) [42]. Compounds **40–44** have approximative HOMO levels at about –4.9 eV. Therefore, besides the oxygen-doping, the poor film formability and the high film conductivity also resulted in the poor FET characteristics of **40–42** [42]. The branched alkyl chains of **43** and **44** not only much enhanced their solubility (>100 mg/mL) that benefits the good film formability, but also moderately decreased their thin-film conductivity (10^{-7}–10^{-8} S/cm), which led to the aforementioned improved FET characteristics. Recently, a series of N-alkyl-substituted bis(pyrrolo[3,4-d])tetrathiafulvalenes (PyTTFs, alkyl = *n*-butyl, *n*-octyl, *n*-dodecyl, *n*-cetyl, and *n*-icosyl, **45–49**, Scheme 6) were synthesized by Takimiya and coworkers as soluble TTF derivatives for solution-processable OFETs [43]. The spin-coated thin films of **45** and **46** showed inferior FET characteristics with mobility of 10^{-5} cm^2/Vs or no reproducible field effect. On the contrary, OFET devices consisting of spin-coated thin films of **47–49** exhibited higher FET performance with mobility about 10^{-2} cm^2/Vs and on/off ratio up to 10^4. The study on solid-state structures of **45–49** by single-crystal analysis and XRD revealed the reason for their different FET performance. Compounds **47–49** formed two-dimensional solid-state structures (columnar π-stacking and intercolumnar S···S interactions), whereas no intermolecular π-stacking feature was observed for **45** and **46**, there were only intermolecular side-by-side S···S interactions. The length of the alkyl chains not only affected the solubility of PyTTFs (very long alkyl groups such as *n*-icosyl chains could reduce solubility), but also influenced their solid-state structures (the long alkyl chains, *n*-dodecyl or longer alkyl groups, led to the two-dimensional solid-state structure) [43].
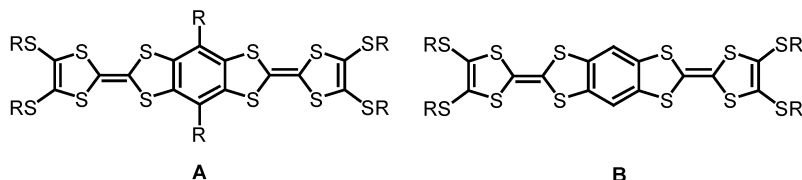
Scheme 7 Two types of benzene-fused bis(tetrathiafulvalene) compounds.
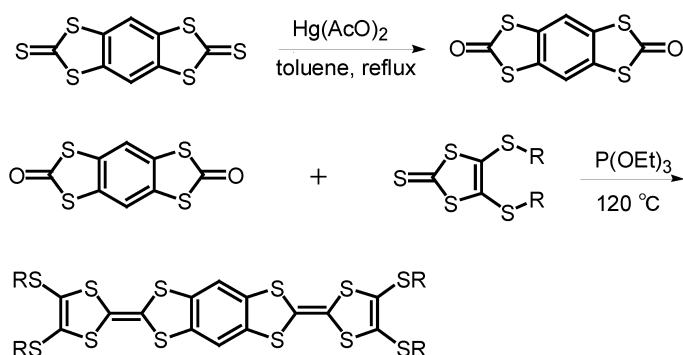
Scheme 8 Synthesis of linear benzene-fused bis(tetrathiafulvalene) compounds. Adapted from ref. [41].
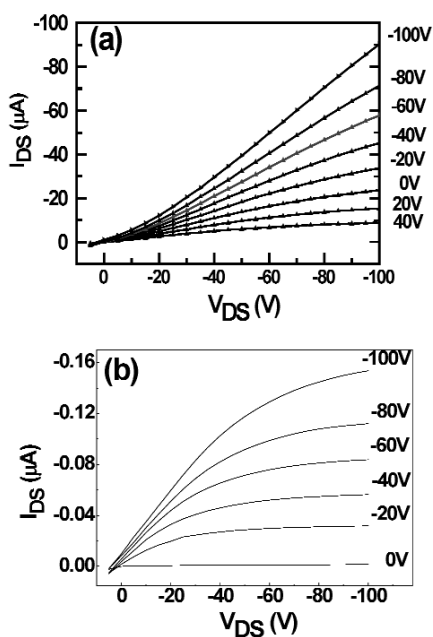
Fig. 7 Output characteristics of thin-film OFETs based on isomeric bis-TTF compounds **41** (a) and **43** (b). Adapted from refs. [41,42], respectively.

Organic charge-transfer compounds containing TTF or its derivatives for OFETs

OCT compounds consisting of TTF or its derivatives, as conducting materials, have been widely investigated in the field of organic conductors and superconductors [7,8]. Recently, OCT compounds comprising TTF or its derivatives have been applied to OFETs [48–54]. They could not only act as single-crystal active layers of OFETs [48–50], but also be used as metallic thin-film electrodes [49–52]. Hasegawa and coworkers reported the ambipolar FET characteristics of devices based on single crystals of OTC compound (BEDT-TTF)(F_2TCNQ) (BEDT-TTF = bis(ethylenedithio)tetrathiafulvalene, F_2TCNQ = 2,5-difluorotetracyanoquinodimethane) [48]. The low-temperature field-effect features showed that ambipolar carrier injection could be achieved down to 2 K. Takahashi et al. first reported that a metallic OTC compound, TTF-TCNQ, could be successfully employed as source and drain electrodes for efficient electron injections in an OFET [49]. Using TTF-TCNQ metallic thin-film electrodes, the OFET based on mixed-stack semiconducting single crystals of OCT compound DBTTF-TCNQ af-

forded high *n*-type mobility up to 1.0 cm^2/Vs [49]. The contact resistance was much smaller in this device than in those with Au or Ag electrodes due to the preferable organic–organic interface. The following work of Takahashi and coworkers demonstrated that organic metal electrodes with different Fermi energy could control *p*-, *n*-, and ambipolar-type carrier injections in OFETs [50]. Three kinds of organic donors (TTF), tetraselenafulvalene (TSF), and DBTTF) and four types of organic acceptors (TCNQ, F$_1$TCNQ, F$_2$TCNQ, and F$_4$TCNQ) were employed to produce conducting OCT films as the electrodes, affording six kinds of OCT electrodes: TTF-TCNQ [A], TTF-F$_1$TCNQ [B], TTF-F$_2$TCNQ [C], TSF-F$_1$TCNQ [D], TSF-F$_2$TCNQ [E], and DBTTF-F$_4$TCNQ [F], with different metal Fermi energy. The aforementioned single crystals of DBTTF-TCNQ acted as the active layers of the prototypical OFET devices. The *n*-type behavior with [A] electrodes changed to ambipolar-type with [C] and [D], and then to *p*-type with [E] and [F]. Mori and coworkers lately reported that pentacene thin-film OFETs with the organic TTF-TCNQ electrodes showed smaller contact resistance and larger overall mobility by more than one order magnitude than those of BC Au electrode transistors [51]. The performance was even comparable to that of TC Au electrodes transistors. In addition, *n*-type organic nanotransistors consisting of TCNQ nanochannel and TTF-TCNQ nanoelectrodes were fabricated by Sakai et al. through co-evaporation method under alternating electric field [52].

CONCLUSION AND OUTLOOK

TTF and its derivatives have gone beyond the field of organic conductors and superconductors, and in recent years, they have been used as semiconducting materials for OFETs. We have summarized the recent progress in the field of TTF-based OFETs. Rovira, Mas-Torrent and their coworkers developed the single-crystal OFETs based on TTF derivatives and precluded the study of TTF-based OFETs. The single-crystal OFETs based on TTF derivatives were fabricated by simple-solution drop-casting method and showed high performance, with the mobility up to 1.4 cm^2/Vs. Although there are many difficulties for the applications of single-crystal OFETs, TTF-based OFETs can be used as models to study the charge transport in TTF-based materials, and the resulting study could afford valuable information for designing and synthesizing new high-performance TTF derivatives. Yamashita et al. did excellent work on vacuum-deposited thin-film OFETs based on TTF derivatives, they also presented effective strategy to obtain high FET performance and stable TTF derivatives. Our group developed two new types of TTF derivatives, linear benzene-fused bis(tetrathiafulvalene) compounds and DB-TTF bisimides, and successfully applied them to solution-processed and vacuum-deposited OFETs, respectively. Takahashi and coworkers successfully employed thin films of OCT compounds containing TTF or its derivatives as source and drain electrodes for efficient charge injections in OFETs. This technique can not only achieve the low-cost electrodes, but also supply the preferable organic–organic interface, and much lower the contact resistance. Up to now, the vacuum-deposited OFETs based on TTF derivatives have shown high performance comparable to that of amorphous silicon, and some of these devices showed good air-stability. However, the mobilities of most solution-processed thin-film OFETs based on TTF derivatives are limited at 10^{-2} cm^2/Vs. We believe that future advances in the field of TTF-based OFETs will go through the design of new TTF species that will be able to combine moderate electron-donating property, planar expanded π-conjugation, and good solubility.

ACKNOWLEDGMENTS

REFERENCES

1. K. E. Katz, Z. Bao, S. Gilat. *Acc. Chem. Res.* **34**, 359 (2001).
2. C. D. Dimitrakopoulos, P. R. L. Malenfant. *Adv. Mater.* **14**, 99 (2002).
3. Y. Sun, Y. Liu, D. Zhu. *J. Mater. Chem.* **15**, 53 (2005).
4. For recent reviews, see special issue "Organic Electronics and Optoelectronics", S. R. Forrest, M. E. Thompson (Eds.). *Chem. Rev.* **107**, 923–1386 (2007).
5. A. Kraft. *ChemPhysChem* **2**, 163 (2001).
6. S. R. Forrest. *Nature* **428**, 911 (2004).
7. J. Ferraris, D. O. Cowan, V. Walatka Jr., J. H. Perlstein. *J. Am. Chem. Soc.* **95**, 948 (1973).
8. For recent reviews, see special issue "Molecular Conductors", P. Batail (Ed.), *Chem. Rev.* **104**, 4887–5782 (2004).
9. M. Mas-Torrent, C. Rovira. *J. Mater. Chem.* **16**, 433 (2006).
10. J. Casado, M. Z. Zgierski, M. C. R. Delgado, J. T. L. Navarrete, M. Mas-Torrent, C. Rovira. *J. Phys. Chem. C* **111**, 10110 (2007).
11. J.-P. Bourgoin, M. Vandevyver, A. Barraud, G. Tremblay, P. Hesto. *Mol. Eng.* **2**, 309 (1993).
12. M. Iizuka, Y. Shiratori, S. Kuniyoshi, K. Kudo, K. Tanaka. *Appl. Surf. Sci.* **130–132**, 914 (1998).
13. M. Mas-Torrent, M. Durkut, P. Hadley, X. Ribas, C. Rovira. *J. Am. Chem. Soc.* **126**, 984 (2004).
14. Naraso, J-i. Nishida, D. Kumaki, S. Tokito, Y. Yamashita. *J. Am. Chem. Soc.* **128**, 9598 (2006).
15. S. M. Sze. *Semiconductor Devices, Physics, and Technology*, p. 490, John Wiley, New York (1985).
16. H. E. Katz, Z. Bao. *J. Phys. Chem. B* **104**, 671 (2000).
17. C. Reese. Z. Bao. *J. Mater. Chem.* **16**, 329 (2006).
18. A. L. Briseno, S. C. B. Mannsfeld, M. M. Ling, S. Liu, R. J. Tseng, C. Reese, M. E. Roberts, Y. Yang, F. Wudi, Z. Bao. *Nature* **444**, 913 (2006).
19. M. Mas-Torrent, P. Hadley, S. T. Bromley, X. Ribas, J. Tarrés, M. Mas, E. Molins, J. Veciana, C. Rovira. *J. Am. Chem. Soc.* **126**, 8546 (2004).
20. M. Mas-Torrent, P. Hadley, S. T. Bromley, N. Crivillers, J. Veciana, C. Rovira. *Appl. Phys. Lett.* **86**, 012110 (2005).
21. M. Mas-Torrent, P. Hadley, X. Ribas, C. Rovira. *Synth. Met.* **146**, 265 (2004).
22. C. Colin, C. R. Pasquier, P. Auban-Senzier, F. Restagno, S. Baudron, P. Batail, J. Fraxedas. *Synth. Met.* **146**, 273 (2004).
23. E. J. Meijer, D. M. De Leeuw, S. Setayesh, E. Van Veenendaal, B.-H. Huisman, P. W. M. Blom, J. C. Hummelen, U. Scherf, T. M. Klapwijk. *Nat. Mater.* **2**, 678 (2003).
24. N. E. Gruhn, D. A. da Silva Filho, T. G. Bill, M. Malagoli, V. Coropceanu, A. Kahn, J.-L. Brédas. *J. Am. Chem. Soc.* **124**, 7918 (2002).
25. (a) S. T. Bromley, M. Mas-Torrent, P. Hadley, C. Rovira. *J. Am. Chem. Soc.* **126**, 6544 (2004); (b) S. T. Bromley, F. Illas, M. Mas-Torrent. *Phys. Chem. Chem. Phys.* **10**, 121 (2008).
26. A. R. Murphy, J. M. J. Fréchet. *Chem. Rev.* **107**, 1066 (2007).
27. Naraso, J-i. Nishida, S. Ando, J. Yamaguchi, K. Itaka, H. Koinuma, H. Tada, S. Tokito, Y. Yamashita. *J. Am. Chem. Soc.* **127**, 10142 (2005).
28. X. Gao, Y. Wang, X. Yang, Y. Liu, W. Qiu, W. Wu, H. Zhang, T. Qi, Y. Liu, K. Lu, C. Du, Z. Shuai, G. Yu, D. Zhu. *Adv. Mater.* **19**, 3037 (2007).
29. B. Noda, H. Wada, K. Shibata, T. Yoshino, M. Katsuhara, I. Aoyagi, T. Mori, T. Taguchi, T. Kambayashi, K. Ishikawa, H. Takezoe. *Nanotechnology* **18**, 424009 (2007).
30. B. Noda, M. Katsuhara, I. Aoyagi, T. Mori, T. Taguchi, T. Kambayashi, K. Ishikawa, H. Takezoe. *Chem. Lett.* **34**, 392 (2005).
31. M. Katsuhara, I. Aoyagi, H. Nakajima, T. Mori, T. Kambayashi, M. Ofuji, Y. Takanishi, K. Ishikawa, H. Takezoe, H. Hosono. *Synth. Met.* **149**, 219 (2005).
32. J. Xue, S. R. Forrest. *Appl. Phys. Lett.* **79**, 3714 (2001).

33. M. Takada, H. Graaf, Y. Yamashita, H. Tada. *Jpn. J. Appl. Phys.* **41**, L4 (2002).
34. Y. Morioka, J.-i. Nishida, E. Fujiwara, H. Tada, Y. Yamashita. *Chem. Lett.* **33**, 1632 (2004).
35. K. Imaeda, Y. Yamashita, Y. Li, T. Mori, H. Inokuchi, M. Sano. *J. Mater. Chem.* **2**, 115 (1992).
36. Y.-L. (Lynn) Loo. *AICHE J.* **53**, 1066 (2007).
37. M. M. Matsushita, H. Kawakami, E. Okabe, H. Kouka, Y. Kawada, T. Sugawara. *Polyhedron* **24**, 2870 (2005).
38. S. Ukai, S. Igarashi, M. Nakajima, K. Marumoto, H. Ito, S. Kuroda, K. Nishimura, Y. Enomoto, G. Saito. *Colloids Surf., A* **284–285**, 589 (2006).
39. P. Miskiewicz, M. Mas-Torrent, J. Jung, S. Kotarba, I. Glowacki, E. Gomar-Nadal, D. B. Amabilino, J. Veciana, B. Krause, D. Carbone, C. Rovira, J. Ulanski. *Chem. Mater.* **18**, 4724 (2006).
40. M. Mas-Torrent, S. Masirek, P. Hadley, N. Crivillers, N. S. Oxtoby, P. Reuter, J. Veciana, C. Rovira, A. Tracz. *Org. Electr.* **9**, 143 (2008).
41. X. Gao, W. Wu, Y. Liu, W. Qiu, X. Sun, G. Yu, D. Zhu. *Chem. Commun.* 2750 (2006).
42. X. Gao, W. Wu, Y. Liu, S. Jiao, W. Qiu, G. Yu, L. Wang, D. Zhu. *J. Mater. Chem.* **17**, 736 (2007).
43. I. Doi, E. Miyazaki, K. Takimiya, Y. Kunugi. *Chem. Mater.* **19**, 5230 (2007).
44. Y. Wang, H. Wang, Y. Liu, C. Di, Y. Sun, W. Wu, G. Yu, D. Zhang, D. Zhu. *J. Am. Chem. Soc.* **128**, 13058 (2006).
45. H. Inokuchi, G. Saito, P. Wu, K. Seki, T. Tang, T. Mori, K. Imaeda, T. Enoki, Y. Higuchi. *Chem. Lett.* 1263 (1986).
46. M. Adam, K. Müllen. *Adv. Mater.* **6**, 439 (1994).
47. K. Lahlil, A. Moradpour, C. Bowlas, F. Menou, P. Cassoux, J. Bonvoisin, J.-P. Launay, G. Dive, D. Dehareng. *J. Am. Chem. Soc.* **117**, 9995 (1995).
48. T. Hasegawa, K. Mattenberger, J. Takeya, B. Batlogg. *Phys. Rev. B* **69**, 245115 (2004).
49. Y. Takahashi, T. Hasegawa, Y. Abe, Y. Tokura, K. Nishimura, G. Saito. *Appl. Phys. Lett.* **86**, 063504 (2005).
50. Y. Takahashi, T. Hasegawa, Y. Abe, Y. Tokura, G. Saito. *Appl. Phys. Lett.* **88**, 073504 (2006).
51. K. Shibata, H. Wada, K. Ishikawa, H. Takezoe, T. Mori. *Appl. Phys. Lett.* **90**, 193509 (2007).
52. M. Sakai, M. Iizuka, M. Nakamura, K. Kudo. *Synth. Met.* **153**, 293 (2005).
53. S. Horiuchi, T. Hasegawa, Y. Tokura. *J. Phys. Soc. Jpn.* **75**, 051016 (2006).
54. S. Horiuchi, T. Hasegawa, Y. Tokura. *Mol. Cryst. Liq. Cryst.* **455**, 295 (2006).